Refractive Index for Atomic Waves: Theory and Detailed Calculations

C. Champenois, E. Audouard, P. Duplàa, Jacques Vigué

Refractive Index for Atomic Waves: Theory and Detailed Calculations

C. Champenois ([1]), E. Audouard ([1,*]), P. Duplàa ([2]) and J. Vigué ([1])

([1]) Laboratoire Collisions, Agrégats, Réactivité ([**]), IRSAMC, Université Paul Sabatier, 118 route de Narbonne, 31062 Toulouse Cedex, France
([2]) Laboratoire de Physique Quantique ([***]), IRSAMC, Université Paul Sabatier, 118 route de Narbonne, 31062 Toulouse Cedex, France

(Received 29 January 1996, revised 21 October 1996, accepted 6 January 1997)

PACS.34.50.-s – Scattering of atoms, molecules, and ions
PACS.03.75.Dg – Atom and neutron interferometry
PACS.34.20.Gj – Intermolecular and atom-molecule potentials and forces

Abstract. — This paper describes new theoretical results and calculations concerning the recently introduced index of refraction of a gas for atomic waves. More precisely, the motion of the atoms of the gas is taken into account and the equation describing the Doppler and Fizeau effects is introduced. The case where the atoms of the wave and the gas have spin 1/2 is also discussed and the rotatory power and circular dichroism of an optically pumped gas is calculated. Finally, the index of the rare gases for sodium waves is calculated. The results show how important it is to take into account glory scattering and Doppler averaging to make a meaningful comparison with experiments. The index appears to be very sensitive to the precise value of the quantum parameter $B = 2\mu D_e \sigma^2$ (in atomic unit). Using the available interaction potential curves, we obtained a reasonably good agreement between the measurements and the corresponding calculated values. However, some experimental results appear difficult to explain with the best available interaction potentials.

Résumé. — Ce travail présente une étude théorique de l'indice de réfraction pour une onde de matière se propageant dans un gaz. Le calcul de l'indice prend en compte le mouvement des atomes du gaz et met en évidence les effets Doppler et Fizeau. Le cas où les atomes du gaz et ceux de l'onde ont un spin 1/2 est également discuté, ce qui permet le calcul du pouvoir rotatoire et du dichroïsme circulaire d'un gaz optiquement pompé. Finalement, l'indice de l'hélium, du néon, de l'argon, du krypton et du xénon est calculé pour une onde de sodium. Ces calculs montrent l'importance des effets de gloire et de la moyenne thermique. Ces effets doivent donc être pris en compte pour l'interprétation précise des résultats expérimentaux. De plus, il apparaît que l'indice dépend fortement du paramètre quantique $B = 2\mu D_e \sigma^2$ (en unité atomique). En utilisant les potentiels sodium–gaz rares disponibles dans la littérature, nous obtenons un accord raisonnable entre l'indice calculé et les résultats expérimentaux. Cependant, il reste difficile de rendre compte de certaines valeurs expérimentales avec les meilleurs potentiels actuellement disponibles.

([*]) Author for correspondence (e-mail: audouard@yosemite.ups-tlse.fr)
([**]) CNRS UMR 5589
([***]) CNRS UMR 5626

1. Introduction

The index of refraction of dilute matter for atomic waves has been recently introduced and measured [1–6]. This index is very interesting because it is an efficient way of interpreting experiments in which a gas is introduced in one arm of an atomic (or molecular) interferometer [1, 2, 6]. It can be also used to evaluate the fundamental limits of atomic interferometry due to the residual gas in the interferometer. Finally, this index is also interesting because it gives a general framework to establish analogies between ordinary optics or neutron optics [7] and atomic optics. A particularly interesting analogy concerns the possibility of developing an amplifier for bosonic atomic waves [4, 8].

The goal of the present paper is twofold:

- we shall first discuss briefly the theory of the index of refraction, with emphasis on the Fizeau Doppler effects. We will also discuss the effects of spins on the atomic wave and in the scattering gas and we will show that a spin polarised gas is a birefringent medium. Finally, we shall use a simple Lennard–Jones potential to discuss the general properties of the index;
- in the second part of this paper, we shall calculate in some detail the index of refraction of He, Ne, Ar, Kr and Xe for Na waves using available potentials. The results are compared to the measurements of references [2] and [6].

2. Theory of the Index of Refraction

We are going to recall firstly the general equations established for the case of fixed scattering centres, and for spinless particles. In a second step, we will discuss the effects due to the motion of the scattering centres, namely the Doppler and Fizeau effects. In a third step, we will discuss the effects of spins and the birefringence of an optically pumped gas.

2.1. Basic Ideas about the Index of Refraction. — We consider here that the atom and the scattering centres have no spins, and that the scattering centres are fixed in the laboratory frame. The scattering of an incident plane wave by one scattering centre at the origin O is described in many textbooks on quantum mechanics [9, 10]:

$$\psi \xrightarrow{r\to\infty} e^{i\mathbf{kr}} + f(\mathbf{k},\mathbf{k}')\frac{e^{i\mathbf{k}'\mathbf{r}}}{r}\cdot \tag{1}$$

The second term is the asymptotic part of the scattered wave in the direction $\mathbf{k}'$. The scattering amplitude f contains all the information on the scattering process.

The connection from the scattering of one centre to the index of refraction n is straightforward [11, 12]. It is made by summing the scattered amplitudes in the forward direction. The result is

$$n = 1 + \frac{2\pi}{k^2} f(\mathbf{k},\mathbf{k}) n_b \tag{2}$$

where $f(\mathbf{k},\mathbf{k})$ is the forward scattering amplitude, noted from now on $f(k)$ and n_b the density of scattering centres. The conditions necessary to establish equation (2) are discussed in reference [12]:

- the atomic wavelength $\lambda = 2\pi/k$ must be considerably smaller than the mean distance between scattering centres $n_b^{-1/3}$ This condition is in fact very weak for atoms at normal

temperatures ($\lambda \approx 10^{-11}$ m);
• collisions must also be independent which means that the potential range must also be smaller than the mean distance $n_b^{-1/3}$. The potential range is of the order of a few 10^{-9} m so that this limits the density more severely.

The propagation of the atomic wave through the gas of index n involves a modified wavevector $\mathbf{k}_m$.

$$\mathbf{k}_m = \mathbf{k} \cdot n. \tag{3}$$

The index is not real and usually the real and imaginary part of $(n-1)$ have comparable magnitudes. The real part describes a modification of the phase velocity of the wave, while the imaginary part describes an attenuation of the wave (this attenuation is well–known as this is just a rewording of the idea of a mean free path) [4].

2.2. Motion of the Scattering Centres. — The fixed scattering centres are now replaced by atoms b of mass m_b and having as a first step all the same velocity $\mathbf{v}_b$. The atomic wave is made of atoms a of mass m_a and velocity $\mathbf{v}_a$. The associated wavevectors are $\mathbf{k}_i = m_i \mathbf{v}_i/\hbar$ $(i = a, b)$. It is easy to describe the scattering process in the centre of mass frame. The centre of mass velocity is $\mathbf{v}_G = (m_a \mathbf{v}_a + m_b \mathbf{v}_b)/(m_a + m_b)$ and the relative velocity is $\mathbf{v}_r = \mathbf{v}_a - \mathbf{v}_b$ with an associated wavevector

$$\mathbf{k}_r = \frac{\mu \mathbf{v}_r}{\hbar} \tag{4}$$

where μ is the reduced mass $\mu = m_a m_b/(m_a + m_b)$. Then, in the centre of mass frame, the index of refraction is

$$n_{CM} = 1 + \frac{2\pi}{k_r^2} f(k_r) n_b \tag{5}$$

and the modified wavevector associated to the relative motion is

$$\mathbf{k}_{rm} = \mathbf{k}_r n_{CM}. \tag{6}$$

Going back to the laboratory frame. we can also define the index n by

$$\mathbf{k}_{am} = \mathbf{k}_a n \tag{7}$$

using the usual relations between the two frames one gets

$$\mathbf{k}_{am} = \mathbf{k}_a + \mathbf{k}_r (n_{CM} - 1) \tag{8}$$

thus, the relation between n and n_{CM} is expressed by

$$\mathbf{k}_a (n-1) = \mathbf{k}_r (n_{CM} - 1). \tag{9}$$

In the general case, $\mathbf{k}_a$ and $\mathbf{k}_r$ are not parallel and the modification of the wavevector is not parallel to $\mathbf{k}_a$. This is a dragging effect, by the motion of the scattering centre. It is related to the Fizeau effect [13] which is also observed with neutrons [14, 15], but usually the treatment of the Fizeau effect neglects the modification of the motion of the scattering centre by the wave, an effect which is taken into account here. The possibility of observing this effect is not established at the present time. In practice, we are first interested by the case of an atomic gas b at thermal equilibrium. Its normalized velocity distribution is given by:

$$P(\mathbf{v}_b) \mathrm{d}^3 \mathbf{v}_b = \frac{1}{\pi^{3/2} \alpha^3} \exp\left(-\frac{\mathbf{v}_b^2}{\alpha^2}\right) \mathrm{d}^3 \mathbf{v}_b \tag{10}$$

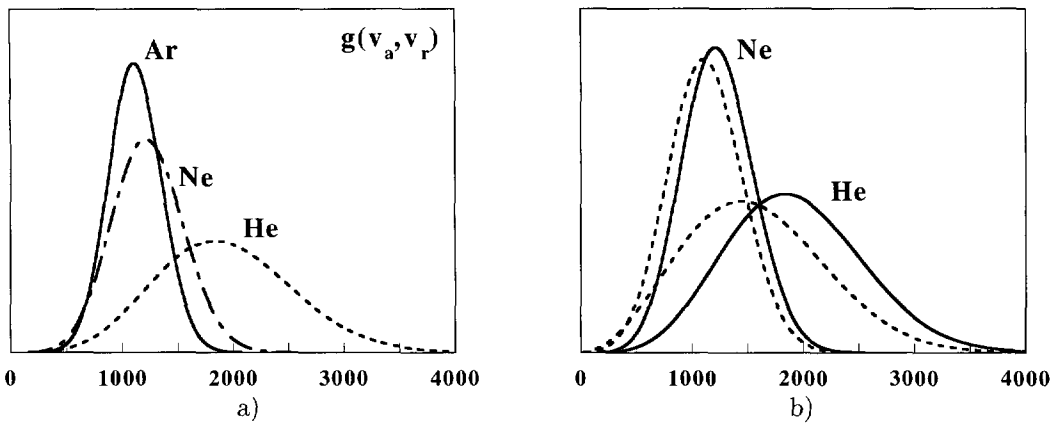

Fig. 1. — a) Weight function $g(v_a, v_r)$ *versus* v_r (in ms^{-1}). The expression of g is given by equation (11b). The sodium wave velocity v_a is taken equal to 1000 ms^{-1} and the gas temperature is $T = 300$ K. The calculation has been made for helium (dot dashed line), neon (broken line) and argon (solid line). b) Comparison of the weight function $g(v_a, v_r)$ (solid line) with the one used in Dalgarno's work [16] (dot dashed line) in the case of helium and neon ($v_a = 1000$ ms^{-1}, $T = 300$ K)

with $\alpha^2 = 2kT/m_b$. T being the temperature of gas b. The modified wavevector $\mathbf{k}_{am}$ is obtained by averaging equation (9) over the distribution $P(\mathbf{v}_b)$. The spherical symmetry of $P(\mathbf{v}_b)$ ensures that $\mathbf{k}_{am}$ and k_a are parallel. The index is a scalar given by:

$$n - 1 = \frac{m_b}{m_a + m_b} \int \frac{2\pi n_b f(k_r)}{k_r^2} g(v_a, v_r) dv_r \tag{11a}$$

where the function $g(v_a, v_r)$ is normalized and given by:

$$g(v_a, v_r) = \frac{2v_r^2}{\alpha\sqrt{\pi}v_a^2} \exp\left(-\frac{v_a^2 + v_r^2}{\alpha^2}\right)\left(\mathrm{ch}\left(\frac{2v_r v_a}{\alpha^2}\right) - \left(\frac{\alpha^2}{2v_r v_a}\right)\mathrm{sh}\left(\frac{2v_a v_r}{\alpha^2}\right)\right). \tag{11b}$$

The function g introduces an important averaging effect, especially in the cases where α is comparable to v_a. In our previous work [5], the weight function g was in error because of an incorrect symmetry assumption. In a preprint of Dalgarno's group [16], the weight function g_d differs from equation (11b) and after conversion in the present notations, it is given by:

$$g_d(v_a, v_r) = \frac{2v_r}{\alpha\sqrt{\pi}v_a} \exp\left(-\frac{v_a^2 + v_r^2}{\alpha^2}\right)\mathrm{sh}\left(\frac{2v_a v_r}{\alpha^2}\right). \tag{12}$$

This difference can be traced back to equation (9) which also appears in this work in a form neglecting the vectorial character of **k**.

Our weight function is plotted in Figure 1a for the cases of a 1000 m/s sodium wave and rare gases (He, Ne, Ar) at 300 K which are representative of the experiments (Ref. [2]). Figure 1b compares our weight function with the one of Dalgarno's group. The difference is very large for a light gas and is particularly important for low v_r values as these functions behave differently like v_r^4 for our function and like v_r^2 for Dalgarno's one.

2.3. Particles with Spins: "Circular Birefringence" of an Optically Pumped Gas. — Birefringence in oriented samples is well-known in neutron optics and has been used

to create polarizing elements [7]. The derivation of the refraction index is completely similar to the derivation in the scalar case. Equation (1) is replaced by:

$$\psi \xrightarrow{r\to\infty} \mathrm{e}^{\imath\mathbf{kr}}|\varphi_0\rangle + S(\mathbf{k},\mathbf{k}')\frac{\mathrm{e}^{\imath\mathbf{k}'\mathbf{r}}}{r}|\varphi_0\rangle \tag{13}$$

where $|\varphi_0\rangle$ describes the initial spin state of the two atoms a and b.

To play a role in the index, a collision must be fully elastic, so that the scattered wave can interfere with the incident wave and thus modify the propagation. This means that the final spin state of both atoms must be identical to the initial state $|\varphi_0\rangle$. The index is then simply given by an equation similar to equation (2):

$$n = 1 + \frac{2\pi}{k^2}\langle\varphi_0|S(\mathbf{k},\mathbf{k})|\varphi_0\rangle n_\mathrm{b}. \tag{14}$$

We will not discuss in this case the Doppler and Fizeau effect, but they obviouslv may be taken into account in a completely similar manner here too.

This expression assumes that the atoms a and b can be both described by a pure spin state. This is not usually the case for the gas b which will be described by a density matrix ρ_b. We calculate the index as a function of the spin state $|\varphi_\mathrm{a}\rangle$ of atom a.

$$n(\varphi_\mathrm{a}) = 1 + \frac{2\pi}{k^2}\langle\varphi_\mathrm{a}|\mathrm{Tr}(S\rho_\mathrm{b})|\varphi_\mathrm{a}\rangle n_\mathrm{b} \tag{15}$$

where $\mathrm{Tr}(S\rho_\mathrm{b})$ is the partial trace over the spin space of atom b. Let us consider a particular case, chosen for its simplicity. The atoms a and b have spins 1/2 and no other angular momentum *i.e.* they are both in a $^2\mathrm{S}_{1/2}$ state. Neglecting any coupling between the molecular $^1\Sigma$ and $^3\Sigma$ states due to fine and hyperfine structure terms, the scattering can be described independently in these two electronic states and the operator S takes the form:

$$S(\mathbf{k},\mathbf{k}') = f^\mathrm{S}(\mathbf{k},\mathbf{k}')P_\mathrm{S} + f^\mathrm{T}(\mathbf{k},\mathbf{k}')P_\mathrm{T} \tag{16}$$

where P_S and P_T are the projectors on the singlet and triplet space, which can be written:

$$\begin{aligned} P_\mathrm{S} &= \frac{1}{4} - \mathbf{s}_\mathrm{a}\mathbf{s}_\mathrm{b} \\ P_\mathrm{T} &= \frac{3}{4} + \mathbf{s}_\mathrm{a}\mathbf{s}_\mathrm{b} \end{aligned} \tag{17}$$

and f^S (resp. f^T) is the singlet (resp. triplet) scattering amplitude.

If the gas b is optically pumped in the state $m_{\mathrm{s_b}} = +1/2$ (the quantization axis may be in any direction of space), the index depends on the spin state $m_{\mathrm{s_a}} = \pm 1/2$ (along the same quantization axis) of the atom of the wave. Its value is given by

$$\begin{aligned} n_+ &= 1 + \frac{2\pi}{k^2} f^\mathrm{T}(k) n_\mathrm{b} \\ n_- &= 1 + \frac{2\pi}{k^2}\left(\frac{1}{2}\right)(f^\mathrm{T}(k) + f^\mathrm{S}(k)) n_\mathrm{b}. \end{aligned} \tag{18}$$

These two indices will usually be different: this is a circular birefringence effect very similar to the rotatory power of a gas or a liquid containing chiral molecules. The analogy is however not fully complete, because at variance with the case of circularly polarized light, here *the spin* quantization axis has no relation with the wavevector direction.

If the atomic wave a enters the gas b in a coherent superposition of the $m_{s_a} = \pm 1/2$ states,

$$|\varphi_a^{in}\rangle = \alpha|+\frac{1}{2}\rangle + \beta|-\frac{1}{2}\rangle \tag{19}$$

after a path of length L, the transmitted beam is in the state

$$|\varphi_a^{out}\rangle = \alpha e^{ikn_+L}|+\frac{1}{2}\rangle + \beta e^{ikn_-L}|-\frac{1}{2}\rangle. \tag{20}$$

The real part of $(n_+ - n_-)$ induces a precession of the spin, while the imaginary part induces a circular dichroism.

The microscopic process has already been studied in the context of scattering experiments of spin exchange collisions [17, 18]. From a more macroscopic point of view, the spin waves predicted and observed in spin polarised gases [19] present interesting similarities.

3. General Properties of the Index of Refraction

The index of refraction of the five rare gases have been measured by the group of Schmiedmayer and Pritchard [2, 3, 6] as a function of the velocity of the sodium beam (in the range $v_a = 750-1750$ m/s) and our discussion will be centered on these cases.

As it is difficult to measure with high accuracy the column density of the rare gas, the most accurate experimental result is the ratio $\rho = \mathrm{Re}(n-1)/\mathrm{Im}(n-1)$ which can be measured without any measurement of the column density. As a consequence our attention will be focused on this ratio ρ. In a first step, we are going to discuss the sensitivity of the index to the main characteristics of the interaction potential $V(r)$ between the rare gas atom and the sodium atom. Although it is well-known that a simple Lennard Jones potential is a rough approximation of the true potential, we will use for this discussion a family of Lennard Jones 6–12 potentials as this is sufficient to understand the main physical ideas. In a second part we will compare the experimental results to calculations involving more realistic potentials whenever they are available.

3.1. The Refractive Index as a Function of the Phase Shifts δ_l. — As is well-known, the forward scattering amplitude is simply expressed as a sum over all the partial waves, and this sum involves the phase shifts δ_l . The real and imaginary parts are given by:

$$\begin{aligned} \mathrm{Im}(f(k_r)) &= \frac{1}{2k_r}\sum_l (2l+1)(1-\cos 2\delta_l) \\ \mathrm{Re}(f(k_r)) &= \frac{1}{2k_r}\sum_l (2l+1)\sin 2\delta_l. \end{aligned} \tag{21}$$

The phase shifts δ_l are deduced from the integration of the Schrödinger equation by Numerov technique [20]. The only particular point upon which we may insist is the fact that the integration must go to very large r values because of the large l involved (l values up to 500–1000). The extraction of the phase shifts is made by comparing the wave to a reference wave calculated in the same way with a vanishing potential.

In Figure 2, we present δ_l as a function of l for three different wavevectors k_r. The shape of this curve is well-known [21, 22], and we present this plot here mostly to discuss the glory effect (see below).

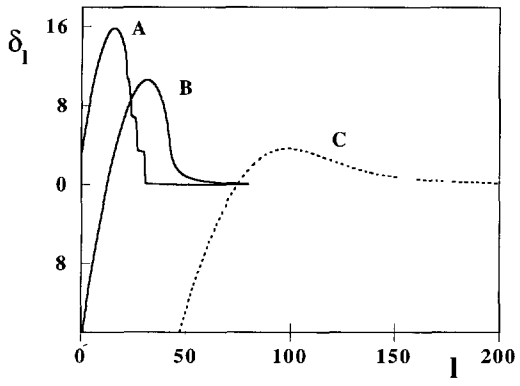

Fig. 2. — Plots of the phase shift δ_l as a function of l for a Lennard–Jones potential ($B = 636$, $\sigma = 8.06$ a.u.). Curve A: $k_r = 2.1 \times 10^{10}$ m^{-1}, curve B: $k_r = 5.5 \times 10^{10}$ m^{-1} and curve C: $k_r = 20.8 \times 10^{10}$ m^{-1}. In the low k_r range, curve A presents jumps of the phase shift equal to π, indication of the existence of resonances while for larger k_r value curves B and C are smooth. All these curves present a maximum leading to the glory effect.

For the very high–l values, we used an asymptotic formula [9]. When the potential at long range is given by a series of inverse r power ($V(r) = -\sum_n \frac{C_n}{r^n}$), this formula is simple:

$$\delta_l^{(\mathrm{app})} = \sum_n \frac{\mu C_n k^{n-2}}{2\hbar^2(1+\frac{1}{2})^{n-1}} \frac{\Gamma\left(\frac{1}{2}\right)\Gamma\left(\frac{n-1}{2}\right)}{\Gamma\left(\frac{n}{2}\right)} . \tag{22}$$

The agreement between the numerical calculations and the asymptotic formula is excellent at large l and we usually switch to this asymptotic formula when δ_l is converging toward zero with $|\delta_l - \delta_l^{(\mathrm{app})}|$ less than 10^{-4} radian.

3.2. Calculation of the Index of Refraction in the Case of a 6–12 Lennard Jones Potential. — These potential curves depend only on two parameters, the well depth D_e and the core radius σ

$$V(r) = 4D_e\left(\left(\frac{\sigma}{r}\right)^{12} - \left(\frac{\sigma}{r}\right)^{6}\right). \tag{23}$$

The collision problem depends on only two dimensionless quantities: the reduced wavevector $A = k_r\sigma$ and the quantum parameter $B = 2\mu D_e\sigma^2$ (in atomic unit). (Here we follow the notations of Bernstein [21]. The very interesting and comprehensive review on elastic scattering by Pauly [23] uses slightly different notations.) This parameter B measures the quantum nature of the atom–atom interaction; the higher B the less quantum is the problem. The number of bound vibrational levels with zero angular momentum scales like $B^{1/2}$ and various authors give rules to predict the number of bound states in a Lennard Jones 6–12 potential well [23–26]. According to reference [23] the critical value of B to have n bound states is obtained by the equation $B_c = 13.93 \times (n - 0.3698)^2$. The critical value for the appearance of one bound level is thus $B_c = 5.53$. From a dimensional analysis, the forward scattering amplitude can be written as a function of a reduced amplitude $f_r(A, B)$:

$$f(k_r) = \sigma f_r(A, B) \tag{24}$$

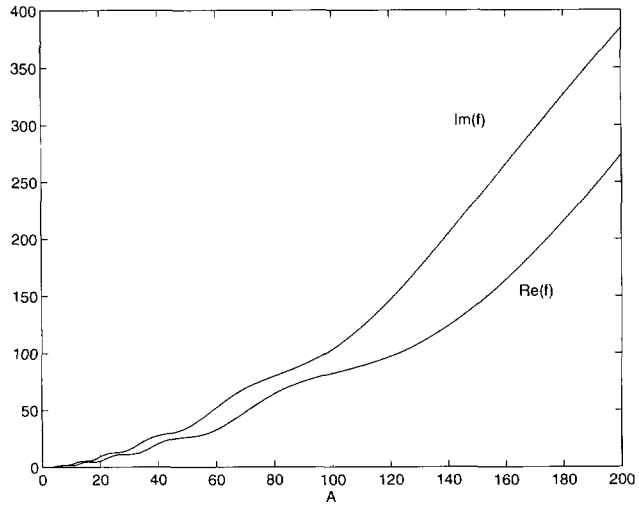

Fig. 3. — Real and imaginary part of the forward scattering amplitude in σ unit *versus* the reduced wavevector A (Lennard–Jones 6–12 potential with $B = 775$).

and the index without velocity averaging is given by:

$$n - 1 = 2\pi n_b \sigma^3 \frac{m_b}{m_a + m_b} f_r(A, B). \tag{25}$$

The scaling of the index is rather complex as it depends linearly on $n_b\sigma^3$ and in a non–linear manner on A and B. We have calculated the forward scattering amplitude for many cases as a function of A and Figures 3 and 4 present typical examples. The real and imaginary parts of f increase with A. This is due to the fact that more and more l values give significant contributions. More interesting are the oscillations of these two quantities with A. They are due to the glory effect. They also appear very clearly on the ratio $\rho = \mathrm{Re}(n-1)/\mathrm{Im}(n-1)$ (also equal to $\mathrm{Re}(f)/\mathrm{Im}(f)$) which is plotted as a function of the reduced wavevector A for various Lennard Jones 6–12 potentials spanning a range of B values from 5 to 775 (Fig. 4). We are now going to discuss the shape of these curves.

First of all, following Bernstein [21] and Pauly [23] there are various ranges of energy:

- the very low energy range, $A^2 < 0.8B$, is the range where the effective potential presents a local minimum which supports quasi–bound states (provided that B is large enough). The scattering amplitude exhibits shape resonances well–described by the Breit–Wigner formula. This energy range has no importance in the experimental data because of the behaviour of the $g(v_a, v_r)$ function for low values of v_r and will not be discussed here but has been briefly discussed in our previous paper [5];

- in the low energy range, when $B < A^2 < B^2$, the scattering amplitude is sensitive to the attractive and repulsive parts of the potential and presents glory oscillations;

- in the high energy range, when $B^2 < A^2$, the scattering amplitude is sensitive almost only to the repulsive wall and the real and imaginary parts of the scattering amplitude are monotonous functions of A.

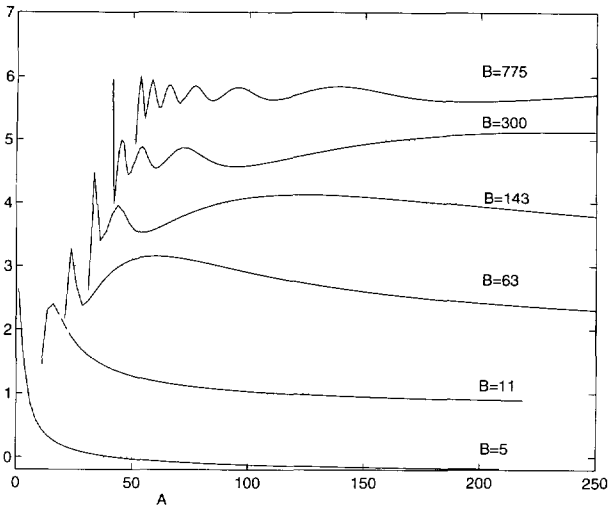

Fig. 4. — Ratio $\rho = \mathrm{Re}(n-1)/\mathrm{Im}(n-1)$ before velocity averaging *versus* the reduced wavevector A. The calculations are made for different Lennard–Jones 6–12 potentials. For each curve, the x–axis is shifted by 10 and the y–axis is shifted by one, and the corresponding B value appears on the top of the curve. The number of glorv oscillations correspond to the number of bound levels ± 1. For the different B values used: 5, 11, 63, 143, 300, 775, the corresponding number of bound levels in the potential is 0, 1, 2, 3, 5, 7.

A simple understanding of the scattering amplitude can be obtained in the following way. Since Massey and Mohr [27], the total scattering cross section has been expressed as a function of the asymptotic behaviour of δ_l for large l values (Eq. (22)). This calculation has been refined by Landau and Lifchitz [9] and gives the imaginary part of f for a potential behaving at long range like r^{-6} by:

$$\mathrm{Im}(f)_{\mathrm{asv}} = 0.7925\sigma A^{3/5} B^{2/5} \tag{26}$$

The ratio ρ of the real and imaginary parts of f can be calculated in the same way and is given for a long range r^{-6} attractive potential by:

$$\rho_{\mathrm{asy}} = \mathrm{Re}(f)_{\mathrm{asv}}/\mathrm{Im}(f)_{\mathrm{asv}} = 0.7265. \tag{27}$$

This calculation has been done for many r^{-n} attractive potential [2] and ρ_{asy} is a function of n, decreasing when n increases ($\rho_{\mathrm{asy}} = 0.4816$ for $n = 8$, $\rho_{\mathrm{asy}} = 0.3640$ for $n = 10$).

In this approximation the phase shifts are large for low l values and the corresponding average values of $\sin 2\delta_l$ and $\cos 2\delta_l$ are equal to zero (Random Phase Approximation). Glory oscillations occur because δ_l as a function of l goes through a maximum as shown in Figure 2. This maximum is related to an undeflected trajectory in the WKB approximation as $\mathrm{d}\delta_l/\mathrm{d}l$ is equal to half the deflection angle in the semiclassical approximation. Then the region of the maximum gives an extra contribution to the sum. This contribution induces the oscillations and one understands easily that these oscillations are out of phase for the real and imaginary part as they involve $\sin 2\delta_l$ and $\cos 2\delta_l$ respectively.

More precisely, following the work of Bernstein [21.28] Pauly [23] and Helbing [29], one can express the glory contribution in the imaginary part of f by a calculation of the sum over l

replaced by an integral calculated in the stationary phase approximation.

$$\mathrm{Im}(f) = \mathrm{Im}(f)_{\mathrm{asy}} + \mathrm{Im}(f)_{\mathrm{gl}} \tag{28a}$$

where

$$\mathrm{Im}(f)_{\mathrm{gl}} = -\mathrm{Im}(f)_{\mathrm{asy}} G(A,B) \cos\left(2\delta_{\mathrm{m}} - \frac{\pi}{4}\right) \tag{28b}$$

where δ_{m} is the maximum of the phase shift and G is the relative amplitude of glory contribution which is a function of the quantum parameter B and the reduced wavevector A. The G function expression is detailed in references [21] and [23]. The same calculation can be done for the real part of f and gives:

$$\mathrm{Re}(f) = \mathrm{Re}(f)_{\mathrm{asy}} + \mathrm{Im}(f)_{\mathrm{asy}} G(A.B) \sin\left(2\delta_{\mathrm{m}} - \frac{\pi}{4}\right). \tag{29}$$

The maximum of the real (imaginary) part is thus reached for $\delta_{\mathrm{m}} = \frac{3}{8}\pi$ ($\delta_{\mathrm{m}} = \frac{5}{8}\pi$) (in both cases modulo π).

An example of the $\mathrm{Im}(f)$ and $\mathrm{Re}(f)$ variation *versus* A is presented in Figure 3 for a B value of 775. The real and imaginary parts of the index are just obtained by a division by k_{r}^2: these two quantities behave roughly like k_{r}^{-1} with superimposed oscillations due to the glory effect.

4. Comparison with Experimental Results for Sodium Waves

4.1. The Potential Curves. — These family of potential curves can be accessed by scattering experiments [30–34] by various types of quantum chemistry calculations [35–44] and finally by laser spectroscopic techniques [45–57].

The scattering experiments give quite accurate information through glory oscillations of the total cross section and rainbow scattering observed in differential experiments. Unfortunately, most of the accurate experiments do not concern alkalis other than sodium.

Ab initio calculations are available in most cases. Such weak van der Waals bonds require special treatments to be described accurately, and the well depth is so small that it is not predicted with great accuracy, with some exceptions like NaNe [37]. However, the long range electronic interaction coefficient $C_n (n = 6, 8, 10)$ have been usually calculated with a good accuracy [39].

Laser spectroscopy experiments give the most accurate description of the interaction potentials. For NaNe [47,50,51,59], NaAr [48,49,52,53,56], NaKr [53,54]. NaXe [55], the study of the A–X transition has given the energies of many rovibrational levels of the X state. From these energies, an accurate description of the well is generally obtained. Moreover, the spectrum of the bound–free emission of the A–X system has been recorded and analysed for a few A levels for NaAr, NaKr, and NaXe [53–56]. The spectral oscillations of these bound free emissions give a very sensitive technique to measure the repulsive wall of the X state potential. Usually a potential has been fitted to all the available data and is expected to give a very accurate description of the X state well and repulsive wall. However these fits are not always fully satisfactory for the calculation of the index of refraction as they do not use a function which connects smoothly to the correct long range behaviour.

For NaHe and NaNe, the measurement of the far red wing of the sodium resonance line perturbed by the corresponding rare gas has been made and interpreted to get the repulsive wall of the X state potential [58,59].

In all the following calculations, the electronic and nuclear spins of the sodium atoms have been forgotten. This is a good approximation because the terms of the Hamiltonian sensitive to

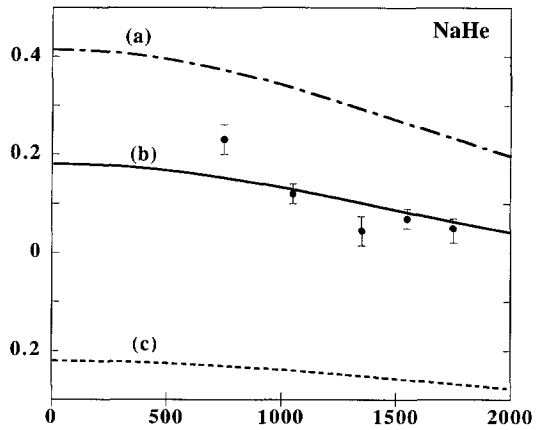

Fig. 5. — Ratio $\rho = \mathrm{Re}(n-1)/\mathrm{Im}(n-1)$ for helium after velocity averaging *versus* sodium velocity v_a (in ms^{-1}). For Figures 5, 6, 7, 8, and 9, the points with error bars are the experimental results of Pritchard's group [2, 6] and the used potentials are described in appendix. Curve (c): Tang–Toennies potential using experimental result of Havey *et al.* [58] and calculated C_n values [39], curve (b): Lennard–Jones potential ($B = 8$), curve (a): Same potential as in curve (c) with modified repulsive wall.

the spin in the alkali–rare gas molecules (spin rotation interaction [60] and hyperfine structure comparable to the atom hyperfine structure) are so small that they play a negligible role during a collision at thermal energy (sudden approximation [10]).

Finally, the sodium atomic beam used in the experiments [2. 6] has a velocity distribution with a relative width $\Delta v/v$ of the order of 3%. This induces a supplementary averaging of the index, which has not been taken into account because it has negligible effects.

4.2. The Refractive Index of Helium for Sodium Atomic Waves. — The case of helium is particular for the following reasons:

i) if the repulsive wall of the NaHe potential is reasonably well–known, there is very little knowledge of the attractive well [41, 44, 58, 61]. It seems clear that this well is very shallow ($D_e \approx 10^{-5}$ a.u. near $r_e \approx 10-12$ a.u.) and can hold at most one bound state. In such a case, the ratio ρ is very small as soon as the wavevector is not too small, and ρ can even be negative as predicted for the limiting case of the hard–sphere potential [2];

ii) the thermal velocity of He at 300 K is large so that the averaging function $g(v_a, v_r)$ is particularly broad and its peak value does not depend much of v_a for low v_a values.

We have built a Tang–Toennies [62] potential with the measured repulsive wing [58] and the calculated long range C_n (Ref. [39]). This attempt is somewhat deceiving: it predicts a too shallow well at a too large r_e value and the corresponding values of the ratio ρ are all negative in clear disagreement with experiment (curve c in Fig. 5). A slightly modified potential with a deeper well was obtained by modifying the repulsive wall in the range $r > 6a_0$. This potential leads to a too high value of the ratio ρ (curve a in Fig. 5).

Therefore, we have made a series of calculations with Lennard–Jones 6–12 potentials although this type of potential curve is not expected to give an accurate representation of the true potential. The ratio ρ for a given velocity depends of B and σ so that a similar agreement can be obtained with various choices. We have arbitrarily fixed $\sigma = 10.02$ a.u. (*i.e.* the value of Pascale and Van de Planque [36]) and the best agreement with the experimental data is

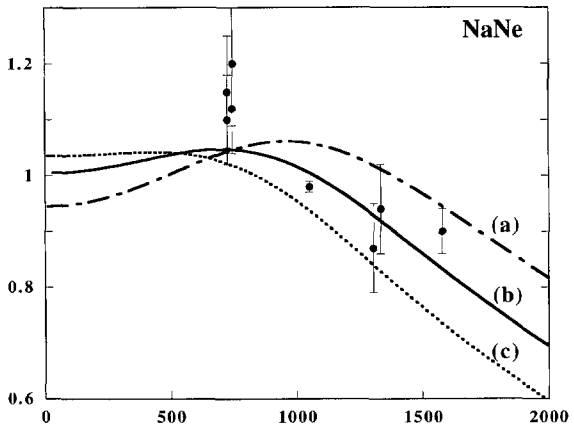

Fig. 6. — Ratio $\rho = \mathrm{Re}(n-1)/\mathrm{Im}(n-1)$ for neon after velocity averaging *versus* sodium velocity v_a (in ms^{-1}). Curve (a): Lennard–Jones 6–12 potential with $B = 110$ ($D_e = 3.7 \times 10^{-5}$ a.u.) [47], curve (b): Lennard–Jones potential with $B = 90$, curve (c): Lennard–Jones potential with $B = 71$.

obtained with $B = 8$, corresponding to the existence of one bound state of the NaHe molecule (a reasonable change of σ by ± 1 a.u. will not modify this conclusion). The agreement between the experimental data points and the calculated curve remains rather poor. As remarked above in (ii), the measured quantity is the result of a broad velocity averaging (the fact that ρ is the ratio of two averaged quantities and not the result of a direct average does not modify this discussion) and the scatter of the experimental data points around a smooth curve cannot be explained by an incorrect shape of the theoretical curve but must be due to some experimental imperfections.

4.3. The Refractive Index of Neon for Sodium Atomic Waves. — The case of neon is somewhat similar to the former case. In this case too, the velocity averaging function g remains very broad and this averaging washes out the first glory oscillations which appear on ρ. Moreover, although the potential curve is better known through laser spectroscopy [47,50,51,59] and *ab initio* calculations [37] no complete potential curve fitting all the available informations has been published.

As a first step, we have made a series of calculations with Lennard–Jones 6–12 potentials. One of these potentials was built so as to have the measured D_e and r_e values ($D_e = 3.69 \times 10^{-5}$ a.u. and $r_e = 10.0$ a.u.) [47]. The two other potentials used have slightly different B values and their σ values were chosen so as to reproduce the calculated long range C_6 coefficient [39]. Figure 6 presents the results of these calculations. The ratio ρ is reasonably well–reproduced, especially by the curve corresponding to $B = 90$. In this case too, none of the calculated curves can be in agreement with all the data point. We find it very difficult to reproduce the first data points ($v_a \approx 750$ m/s) with any reasonable choice of potential, and like in the case of helium, the broad velocity average makes it impossible to reproduce well at the same time the first two set of data points ($v_a = 750$ m/s and $v_a = 1050$ m/s). If we forget the $v_a = 750$ m/s first data points, the three other ones are rather well–represented by the $B = 90$ curve and the agreement would be improved by the choice of a slightly larger B value. We do not think that this improvement would be meaningful because of the limitations of the Lennard–Jones potential.

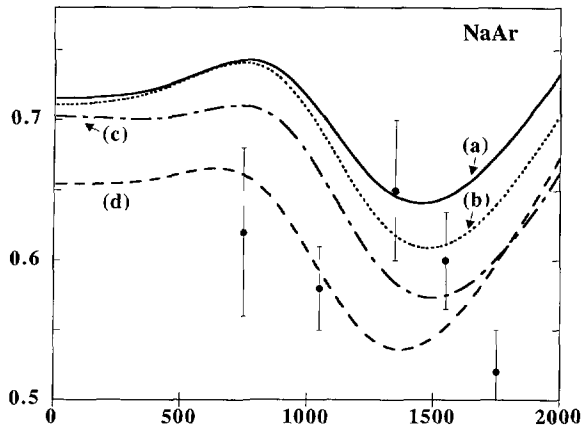

Fig. 7. — Ratio $\rho = \mathrm{Re}(n-1)/\mathrm{Im}(n-1)$ for argon after velocity averaging *versus* sodium velocity v_a (in ms^{-1}). Curve (a): Lennard–Jones 6–12 potential with $B = 775$, curve (b): HFD potential proposed by Zimmermann [56], curve (c): potential proposed by Düren [33], curve (d): potential proposed by Tellinghuisen [49] and modified according reference [5].

4.4. The Refractive Index of Argon for Sodium Atomic waves. — The case of argon is very different from the previous ones. Because of the larger value of D_e ($D_e = 1.84 \times 10^{-4}$ a.u.) [49] and of the reduced mass, the quantum parameter B is considerably larger ($B \approx 700$) and the potential holds a series of bound states (the estimated value of the fractional quantum number at dissociation [49] is $v_D = 6.67$). Before velocity averaging, the ratio ρ exhibits a series of glory oscillations as shown in Figure 4.

The spectroscopy of this ground state has been the subject of many efforts and several potential curves are available [33, 49, 53, 56] which have been deduced from high quality fits to experimental data. Using these potential curves (for the one of Ref. [49], we have corrected its long range behaviour in a way described in Ref. [5]) and a Lennard Jones potential ($B = 775$), we have calculated the curves presented in Figure 7. The glory oscillations are almost completely washed out by the velocity averaging, but the remaining oscillations patterns are very similar for the four different potential curves, and unfortunately they do not fit the oscillation which appears on the experimental data. As shown in Figure 4, changing the well depth changes the phase of the glory oscillations. But the change required to fit the experimental results is considerably larger than the claimed accuracy of the measurements of the well depth. It is interesting to remark that the curve deduced by us from reference [49] and having a correct long range behaviour with r^{-6}, r^{-8} and r^{-10} terms gives lower ρ values than the other curves which behave like r^{-6} These lower ρ values are expected from the asymptotic behaviour of the phase shifts and they are also in better agreement with the measurements.

4.5. The Refractive Index of Krypton for Sodium Atomic Waves. — As in the case of argon, the potential well is deep enough to hold several bound levels. The same number (± 1) of glory oscillations are then observed in the ratio ρ before velocity averaging, but although the velocity averaging function is substantially narrower than for argon, only the last two oscillations survive to the velocity averaging. We have used the potential provided by Zimmermann's group [54]. We have also built a Lennard–Jones potential using D_e value deduced from the experimental results ($D_e = 3.11 \times 10^{-4}$ a.u.). The extra r^{-8} and r^{-10} long range terms of the experimental potential explain the difference between the two asymptotic values of ρ for small

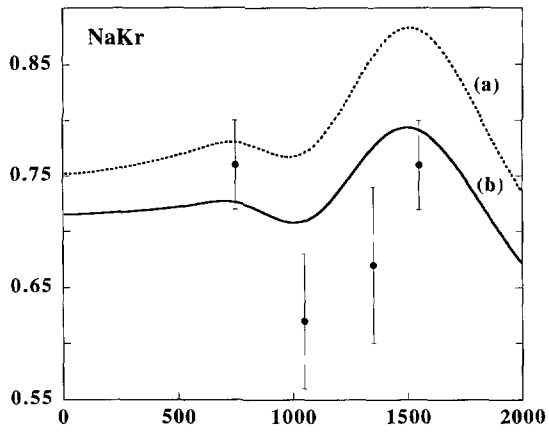

Fig. 8. — Ratio $\rho = \mathrm{Re}(n-1)/\mathrm{Im}(n-1)$ for krypton after velocity averaging *versus* sodium velocity v_a (in ms^{-1}). Curve (a): HFD potential proposed by Zimmermann [54], curve (b): Lennard–Jones 6–12 potential with $B = 1732$.

incident velocities and the difference of the shape of the curves. Unfortunately, the C_8 term used in reference [54] has a negative unphysical value. The measured values of ρ also plotted in Figure 8 are in poor agreement with the calculated values. So the used potentials seem not to describe properly the sodium–krypton interactions on the whole range of internuclear distance.

4.6. The Refractive Index of Xenon for Sodium Atomic Waves. — The xenon case is similar to the two previous ones (heavier atoms). As in the krypton case, we used the potential given by Zimmermann [55], and a Lennard Jones potential built on the experimental results of the same authors ($D_e = 5.3 \times 10^{-4}$ a.u.). In this case, the experimental potential do not take into account r^{-8} or r^{-10} terms and, as shown in Figure 9, the asymptotic values of the ratio ρ for low velocity are the same and are very close to 0.7265 as expected (see Sect. 3.2). Actually, the two potentials have the same long range behaviour but differ in short range since the repulsive wall of the Zimmermann potential is exponential. However the two corresponding ρ curves have almost the same shape but they cannot fit all the measurements: only three out of five data points are close to the calculated curves, and the first point has a very large error bar. These preliminary results point out the need for more accurate potentials and index measurements.

5. Conclusion

In this paper, we have further developed the theory of the refractive index of a gas for atomic waves and we have made an application of this theory to interpret the recently measured values of the index of helium, neon and argon for sodium waves.

In the theoretical developments, we have considered the effect of the motion of the atom of the gas on the index. The basic equation describing the atomic analogs of the Doppler and Fizeau effects has been established. We have also considered the case where the two atoms (the wave and the component of the gas) both have a spin 1/2. An optically pumped gas thus presents rotatory power and dichroism for the atomic wave, in analogy with optics. The corresponding index which has then a simple tensorial character has been evaluated. A generalization to higher spins seems rather simple, but this will imply a richer tensorial nature.

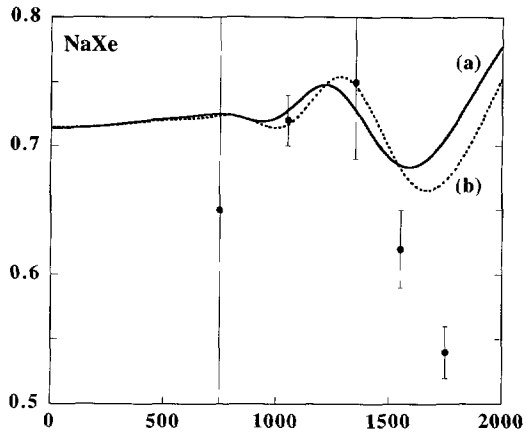

Fig. 9. — Ratio $\rho = \mathrm{Re}(n-1)/\mathrm{Im}(n-1)$ for xenon after velocity averaging *versus* sodium velocity v_a (in ms^{-1}). Curve (a): Lennard-Jones 6-12 potential with $B = 2566$, curve (b): HFD potential proposed by Zimmermann [55].

The evaluation of the index of helium, neon, argon, krypton and xenon for sodium waves has shown very clearly the importance of glory scattering: this effect appears exceptionally well on the quantity of greatest experimental interest, namely the ratio $\rho = \mathrm{Re}(n-1)/\mathrm{Im}(n-1)$. This quantity is also highly sensitive to the fact that the thermal averaging effect is taken into account. Finally, the case of helium differs noticeably from the other cases. The available potential is not as accurate, but the measured value of the ratio ρ gives a sensitive test of the presence or the absence of one bound state for the NaHe molecule.

Acknowledgments

Funding of our laboratories by the "Région Midi-Pyrénées" is gratefully acknowledged. G. Peach and D. Zimmermann have kindly given us information on the potentials. We thank J. Schmiedmayer for the communication of reference [6] prior to publication.

Appendix

Potentials Used in the Index Calculations (Values in Atomic Unit)

A.1. NaHe

A.1.1. Tang and Toennies [62] Potentials Based on the Measurements of Reference [58] and on Calculated Long Range C_n Coefficients (Ref. [39])

i) curve (c) in Figure 5:

$$V(r) = A\mathrm{e}^{-br} - \frac{C_6}{r^6} f_6(r) - \frac{C_8}{r^8} f_8(r) - \frac{C_{10}}{r^{10}} f_{10}(r)$$

with

$$f_{2n}(r) = 1 - \left(\sum_{k=0}^{2n} \frac{(br)^k}{k!} \right) \mathrm{e}^{-br}$$

ii) modified potential, curve (a) in Figure 5:
Ae^{-br} is replaced by $A\exp(-br - c(r - r_0)^2)$ for $r > r_0$

Constant	Value	Value modified pot.	Ref.
C_6	24.4	24.4	[39]
C_8	1329	1329	[39]
C_{10}	87 538	87 538	[39]
A	0.278 16	0.278 16	[58]
b	0.799	0.785	[58]
c		0.15	
r_0		6	
D_e	9.70×10^{-7}	1.46×10^{-5}	

A.1.2. Lennard–Jones 6- 12 Potential (Curve (b) in Fig. 5)

Constant	Value	Ref.
B	8	
σ	10.02	[36]
D_e	6.4×10^{-6}	

A.2. NaNe

A.2.1. Lennard–Jones 6–12 Potential (cf. Fig. 6)

Constant B	σ	D_e
Curve (a) 110	8.9	3.7×10^{-5} [47]
Curve (b) 90	8.5	3.1×10^{-5}
Curve (c) 71	8.3 [39]	2.6×10^{-5}

A.3. NaAr

A.3.1. Lennard–Jones 6–12 Potential (Curve (a) in Fig. 7)

Constant	Value
B	775
σ	8.4
D_e	2.0×10^{-4}

A.3.2. Potential Fitted by Zimmermann et al. [56] to Spectroscopic Results (Curve (b) in Fig. 7)

$$V(r) = Ae^{-br} - f(r)\left(\frac{C_6}{r^6} + \frac{C_8}{r^8} + \frac{C_{10}}{r^{10}}\right)$$

$$f(r) = \exp\left(-\left(\left(\frac{r_c}{r}\right)^m - 1\right)^2\right) \qquad r < r_c$$

$$f(r) = 1 \qquad r > r_c,$$

with the following values of the parameters

C_6	C_8	C_{10}	A	b	m	r_c	D_e	r_e
194	119 215	0	3.58×10^{-2}	0.468	1	19.98	1.91×10^{-4}	9.48

A.3.3. Potential Proposed by Düren et al. [33] (Curve (c) in Fig. 7)

The potential equation is expressed in reference [33]. The values of the well depth and equilibrium distance are $D_e = 1.95 \times 10^{-4}$ and $r_e = 9.54$.

A.3.4. Potential Used in our Previous Work [5] (Curve (d) in Fig. [7]). — This potential is the one proposed by Tellinghuisen [49] slightly modified for the long range behaviour according to reference [5] ($D_e = 1.84 \times 10^{-4}$).

A.4. NaKr

A.4.1. HFD Potential Proposed by Zimmermann et al. [56]: (Curve (a) in Fig. 8)

Same equations as in 3.2 with following parameters:

C_6	C_8	C_{10}	A	b	m	r_c	D_e	r_e
772.6	−71 384	31 269 560	6.306	1.278	2	12.042	3.11×10^{-4}	9.29

A.4.2. Lennard Jones 6–12 Potential (Curve (b) in Fig. 8)

Constant	Value	Ref.
B	1732	
σ	9.2	
D_e	3.1×10^{-4}	[54]

A.5. NaXe

A.5.1. Lennard Jones 6–12 Potential (Curve (a) in Fig. 9)

Constant	Value	Ref.
B	2566	
σ	8.2	
D_e	5.3×10^{-4}	[55]

A.5.2. HFD–Potential Proposed by Zimmermann et al. [55]: (Curve (b) in Fig. 9)

Same equations as in 3.2 with the following values of the parameters

C_6	C_8	C_{10}	A	b	m	r_c	D_e	r_e
662.4	0	0	26.853	1.446	2	12.36	5.29×10^{-4}	9.37

References

[1] Schmiedmayer J., Ekstrom C.R., Chapman M.S., Hammond T.D. and Pritchard D.E., Fundamentals of Quantum optics III, Lectures Notes in Physics 420, F. Ehlotzky, Ed. (Springer) p. 21.
[2] Schmiedmayer J., Chapman M.S., Ekstrom C.R., Hammond T.D., Wehinger S. and Pritchard D.E., *Phys. Rev. Lett.* **74** (1995) 1043.
[3] Chapman M.S., Ekstrom C.R., Hammond T.D., Rubenstein R.A., Schmiedmayer J., Wehinger S. and Pritchard D.E., *Phys. Rev. Lett.* **74** (1995) 4783.
[4] Vigué J., *Phys. Rev. A* **52** (1995) 3973.
[5] Audouard E., Duplàa P. and Vigué J., *Europhys. Lett.* **32** (1995) 397.
[6] Schmiedmayer J. *et al.*, review paper (to be published).
[7] Sears V., Neutron optics (Oxford University Press, 1989).
[8] Bordé Ch.J., *Phys. Lett. A* **204** (1995) 217.
[9] Landau L. and Lifchitz E., Quantum Mechanics (Pergamon Press, 1965).
[10] Messiah A., Mécanique Quantique (Dunod, 1969).
[11] Fermi E., Nuclear Physics (University of Chicago Press, 1950).
[12] Newton R.G., Scattering theory of waves and particles (Mc Graw–Hill, 1966).
[13] Fizeau M.H., *C. R. Hebd. Seances Acad. Sci.* **33** (1851) 349; Fizeau H.L., *Ann. Chim. Phys.* **57** (1859) 385.
[14] Bonse U. and Rumpf A., *Phys. Rev. Lett.* **56** (1986) 2441.
[15] Horne M.A., Zeilinger A., Klein A.G. and Opat G., *Phys. Rev. A* **28** (1983) 1.
[16] Forrey R.C., You L., Kharchenko V. and Dalgarno A., *Phys. Rev. A* **54** (1996) 2180.
[17] Balling C., Hanson R.J. and Pipkin F.M., *Phys. Rev. A* **133** (1964) 607.
[18] Berlinsky A.J. and Shizgal B., *Can. J. Phys.* **58** (1980) 88.
[19] Lhuillier C. and Laloë F., *J. Phys. France* **43** (1982) 197; 225.
[20] Cashion J.K., *J. Chem. Phys.* **39** (1963) 1872.
[21] Bernstein R.B., *J. Chem. Phys.* **38** (1963) 2599.
[22] Levine R.D. and Bernstein R.B., Molecular Reaction Dynamics and Chemical Reactivity (Oxford University Press, 1987).
[23] Pauly H., in Atom–molecule collision theory, R.B. Bernstein, Ed. (Plenum, 1979) p. 111.
[24] Bernstein R.B., *J. Chem. Phys.* **37** (1962) 1880.
[25] Harrison H. and Bernstein R.B., *J. Chem. Phys.* **38** (1963) 2135.
[26] Cashion J.K., *J. Chem. Phys.* **48** (1967) 94.
[27] Massey H.S.W. and Mohr C.B.O., *Proc. Roy. Soc. (London) A* **144** (1934) 188.
[28] Bernstein R.B., *J. Chem. Phys.* **37** (1969) 1880.
[29] Helbing R.K.B., *J. Chem. Phys.* **50** (1969) 493.
[30] Buck U. and Pauly H., *Z. Phys.* **208** (1968) 390.
[31] Düren R., Raabe G.P. and Schlier Ch., *Z. Phys.* **214** (1968) 410.
[32] Düren R., Frick A. and Schlier Ch., *J. Phys B* **5** (1972) 1744.
[33] Düren R. and Gröger W., *Chem. Phys. Lett.* **56** (1978) 67.
[34] Feltgen R., Kirst H., Kölher A., Pauly H. and Torello F., *J. Chem. Phys.* **76** (1982) 2360.
[35] Baylis W.E., *J. Chem. Phys.* **51** (1969) 2665.
[36] Pascale J. and Van de Planque J., *J. Chem. Phys.* **60** (1974) 2278.
[37] Masnou F., Phillipe M. and Valiron P., *Phys. Rev. Lett.* **41** (1976) 395.
[38] Saxon R.P., Olson R.E. and Liu B., *J. Chem. Phys.* **67** (1977) 2692.
[39] Tang K.T., Norbeck J.M. and Certain P.R., *J. Chem. Phys.* **64** (1976) 3063; Standard J. and Certain P., *J. Chem. Phys.* **83** (1985) 3002.
[40] Laskowski B.C., Langhoff S.R. and Stallcop J.R., *J. Chem. Phys.* **75** (1981) 815.

[41] Pontius E.M. and Sando K.M., *Phys. Rev. A* **28** (1983) 3117.
[42] Czuchaj E., Rebentrost F., Stoll H. and Preuss H., *Chem. Phys.* **136** (1989) 79.
[43] Czuchaj E., Rebentrost F., Stoll H. and Preuss H., *Chem. Phys. Lett.* **173** (1990) 573.
[44] Theodorakopoulos G. and Petsalakis I.D., *J. Phys. B* **26** (1993) 4367.
[45] Carrington C.G., Drummond D., Gallagher A. and Phelps A.V., *Chem. Phys. Lett.* **22** (1973) 511.
[46] York G., Scheps R. and Callagher A;, *J. Chem. Phys.* **63** (1975) 1052.
[47] Ahmad Bitar R., Lapatovich W.P. and Pritchard D.E., *Phys. Rev. Lett.* **39** (1977) 1657.
[48] Smalley R.E., Auerbach D.A., Fitch P.S., Levy D.H. and Wharton L., *J. Chem. Phys.* **66** (1977) 3778; Goble J.H. and Winn J.S., *J. Chem. Phys.* **70** (1979) 2051.
[49] Tellinghuisen J., Ragone A., Kim M.S., Auerbach D.J., Smalley R.E., Wharton L. and Levy D.H., *J. Chem. Phys.* **71** (1979) 1283.
[50] Lapatovich W.P., Ahmad-Bitar R., Moskowitz P.E., Renhorn I., Gottscho R.A. and Pritchard D.E., *J. Chem. Phys.* **73** (1980) 5419.
[51] Gottscho R.A., Ahmad-Bitar R., Lapatovich W.P., Renhorn I. and Pritchard D.E. , *J. Chem. Phys.* **75** (1981) 2546.
[52] Aepfelbach G., Nunnemann A. and Zimmerman D., *Chem. Phys. Lett.* **96** (1983) 311.
[53] Zimmermann D., *Acta Physica Hungarica* **67** (1990) 351.
[54] Brühl R., Kapenatis J. and Zimmermann D., *J. Chem. Phys.* **94** (1991) 5865.
[55] Baumann P., Zimmermann D. and Brühl R., *J. Mol. Spec.* **155** (1992) 277.
[56] Zimmermann D., private communication (1996).
[57] Kumar M., Rai S.B. and Rai D.K., *Nuovo Cimento* **15** (1993) 1445.
[58] Havey H.D., Frolking S.E. and Wright J.J., *Phys. Rev. Lett.* **45** (1980) 1783.
[59] Havey H.D., Frolking S.E., Wright J.J. and Balling L.C., *Phys. Rev. A* **24** (1981) 3105.
[60] Bouchiat C., Bouchiat M. and Pottier L., *Phys. Rev.* **181** (1969) 1444.
[61] Peach G., private communication (1996).
[62] Tang K. and Toennies J.P, *J. Chem. Phys.* **80** (1984) 3726.